Pure Spin Current Injection in Hydrogenated Graphene Structures

Reinaldo Zapata-Peña, Bernardo S. Mendoza, Anatoli I. Shkrebtii

1 Introuction

sec:introuction

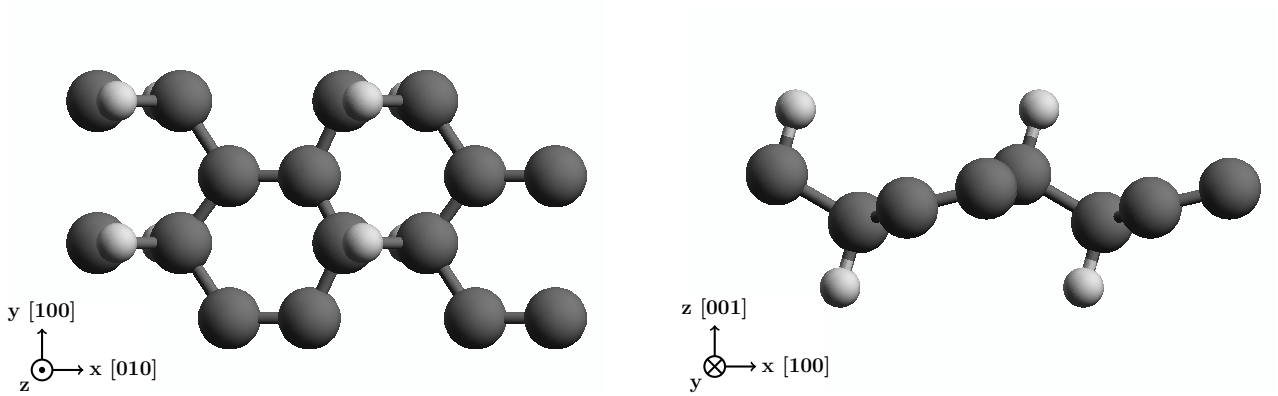

Figure 1: Alt structure.

fig:altstruc

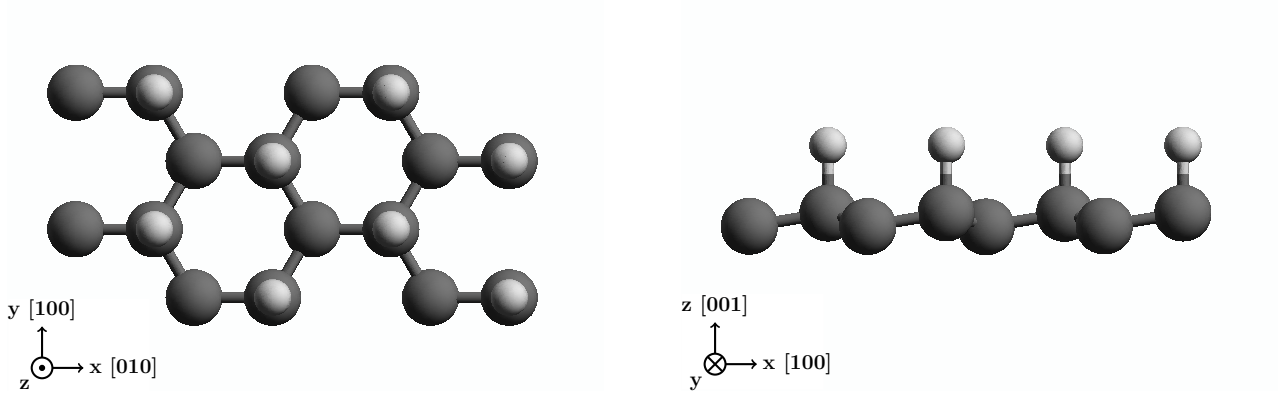

Figure 2: Up structure

fig:upstruc

2 Theory

sec:theory

The equation for $\mathcal{V}^{\mathrm{ab}}$ for normal incidence in the xy plane is given by

$$\begin{aligned}\mathcal{V}^{\mathrm{ab}}(\omega) &= \frac{\mu^{\mathrm{abxx}}(\omega)E^2(\omega)\cos^2\theta + \mu^{\mathrm{abyy}}(\omega)E^2(\omega)\sin^2\theta + 2\mu^{\mathrm{abxy}}(\omega)E^2(\omega)\cos\theta\sin\theta}{\xi^{\mathrm{xx}}(\omega)E^2(\omega)\cos^2\theta + \xi^{\mathrm{yy}}(\omega)E^2(\omega)\sin^2\theta}, \\ &= \frac{\mu^{\mathrm{abxx}}(\omega)\cos^2\theta + \mu^{\mathrm{abyy}}(\omega)\sin^2\theta + 2\mu^{\mathrm{abxy}}(\omega)\cos\theta\sin\theta}{\xi^{\mathrm{xx}}(\omega)\cos^2\theta + \xi^{\mathrm{yy}}(\omega)\sin^2\theta}. \end{aligned} \tag{1}$$

eq:vab

For an angle $\theta = \frac{\pi}{4}$ this expression can be reduced to

$$\mathcal{V}^{\mathrm{ab}}(\omega) = \frac{\mu^{\mathrm{abxx}}(\omega) + \mu^{\mathrm{abyy}}(\omega) + 2\mu^{\mathrm{abxy}}(\omega)}{\xi^{\mathrm{xx}}(\omega) + \xi^{\mathrm{yy}}(\omega)}. \tag{2}$$

eq:vab-90deg

We also define $|\mathcal{V}^{\mathrm{a}}|$ as

$$|\mathcal{V}^{\mathrm{a}}| = \sqrt{(\mathcal{V}^{\mathrm{ax}})^2 + (\mathcal{V}^{\mathrm{ay}})^2 + (\mathcal{V}^{\mathrm{az}})^2}, \tag{3}$$

eq:vab-mag

and the corresponding polar and azimuthal angles θ and φ as

$$\theta = \cos^{-1}\left(\frac{\mathcal{V}^{\mathrm{az}}}{|\mathcal{V}^{\mathrm{a}}|}\right), \qquad 0 \leq \theta \leq \pi, \tag{4}$$

eq:polar-ang

$$\varphi = \tan^{-1}\left(\frac{\mathcal{V}^{\mathrm{ay}}}{\mathcal{V}^{\mathrm{ax}}}\right), \qquad 0 \leq \varphi \leq 2\pi. \tag{5}$$

eq:azimuthal-ang

(6)

3 Results

sec:results

We preset the results for $\mathcal{V}^{\mathrm{ab}}$ for the $C_{16}H_8$-alt and $C_{16}H_8$-up structures being both noncentrosymmetric semi-infinite carbon systems with 50% hydrogenation in different arrangements. The *alt* system has alternating hydrogen atoms on the upper and bottom sides of the carbon sheet, while the *up* system has H only on the upper side. We take the hexagonal carbon lattice to be on the xy plane for both structures, and the carbon-hydrogen bonds on the perpendicular xz plane, as depicted in Figs. 1 and 2.

Using the ABINIT code [1] we calculated the self- consistent ground state and the Kohn-Sham states using density functional theory in the local density approximation (DFT-LDA) with a planewave basis. We used Hartwigsen-Goedecker-Hutter (HGH) relativistic separable dual-space Gaussian pseudopotentials [2] including the spin-orbit interaction for calculating $\mathcal{V}^{\mathrm{a}}(\omega)$.

The convergence parameters for the calculations of our results corresponding to the *alt* and *up* structures are cutoff energies of 65 Ha and 40 Ha, respectively. The energy eigenvalues and matrix elements were calculated using 14452 **k** points and 8452 **k** points in the irreducible Brillouin zone (IBZ) and present LDA energy band gaps of 0.72 eV and 0.088 eV, respectively for the *alt* and *up* structures. As mentioned in [4], using DFT the LDA is only one method of many other that can be used to calculate the electronic structure of materials. Also it is known that all methods predict a different band gap than the obtained in the experiment. A correction for the band gap energy value can be calculated by other *ab-initio* methods such as the GW approximation [3] being this outside the scope of this paper.

The structures presented here where divided into layers to analyze the he layer- by-layer contribution for $\mathcal{V}^{\mathrm{ab}}$ response. The *alt* structure was divided in six layers corresponding the first one to the top hydrogen atoms, from the second to the forth to carbon atoms in different z positions, and the sixth and last one to the bottom hydrogen atoms. The *up* structure was divided into two layers, the first one comprised by the top hydrogen atoms and the second by the carbon atoms. The layer divisions and atom positions for the unit cells are shown in Tables 1 and 2.

Table 1: Unit cell of *alt* structure.

tab:altunitcell

Layer No.	Atom type	Position [Å]		
		x	y	z
1	H	-0.61516	-1.42140	1.47237
2	C	-0.61516	-1.73300	0.39631
3	C	0.61516	1.73300	0.15807
4	C	0.61516	0.42201	-0.15814
5	C	-0.61516	-0.37396	-0.39632
6	H	-0.61516	-0.68566	-1.47237

Layer division, atom types and positions for the *alt* structure. The structure unit cell was divided in six layers corresponding each one to atoms in different z positions.

Table 2: Unit cell of *up* structure.

tab:upunitcell

Layer No.	Atom type	Position [Å]		
		x	y	z
1	H	-0.61516	-1.77416	0.73196
1	H	0.61518	0.35514	0.73175
2	C	-0.61516	-1.77264	-0.49138
2	C	-0.61516	-0.35600	-0.72316
2	C	0.61516	0.35763	-0.49087

Layer division, atom types and positions for the *up* structure. The structure unit cell was divided in two layers corresponding to hydrogen and carbon atoms.

3.1 alt

sec:results-alt

3.1.1 $\mathcal{V}^{\mathrm{xb}}$

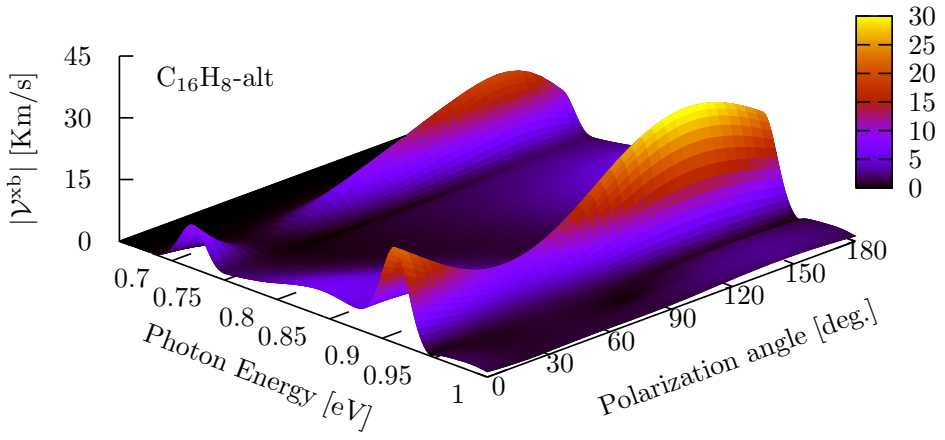

Figure 3: The most intense response for $\mathcal{V}^{\mathrm{xb}}$ is for 145°.

fig:alt-magvxbincang

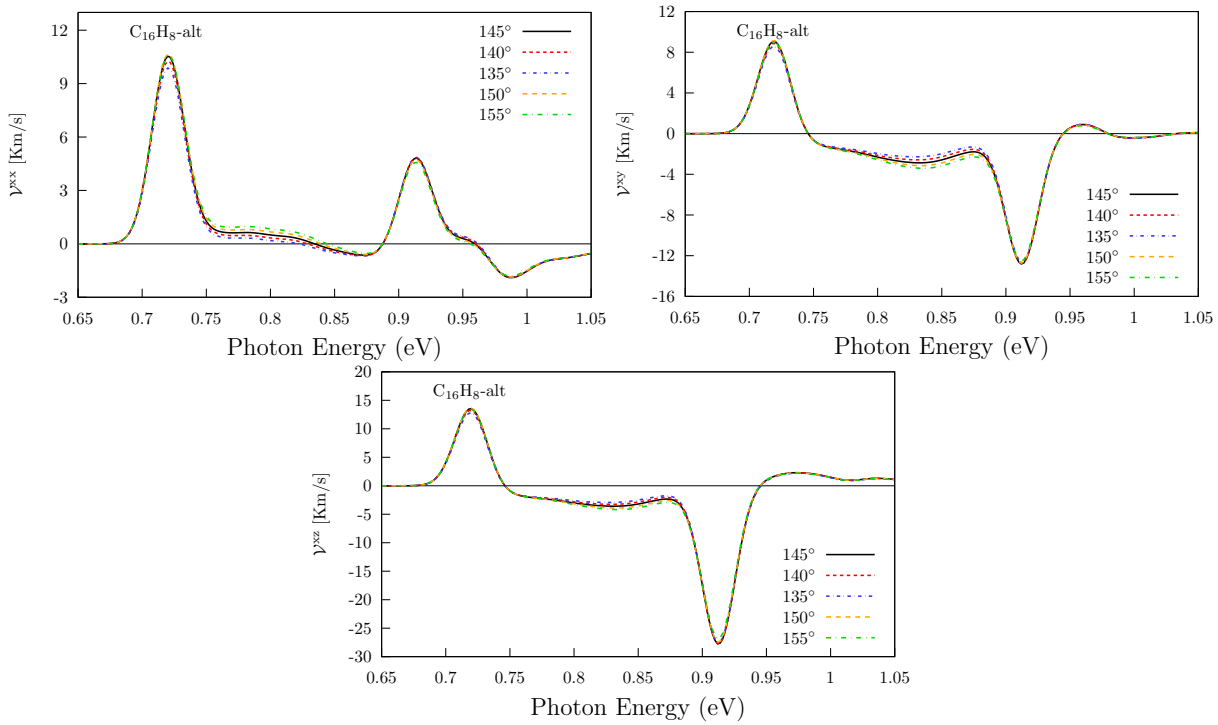

Figure 4: Cheking angle of incidence for xb components. fig:alt-xbangcomp

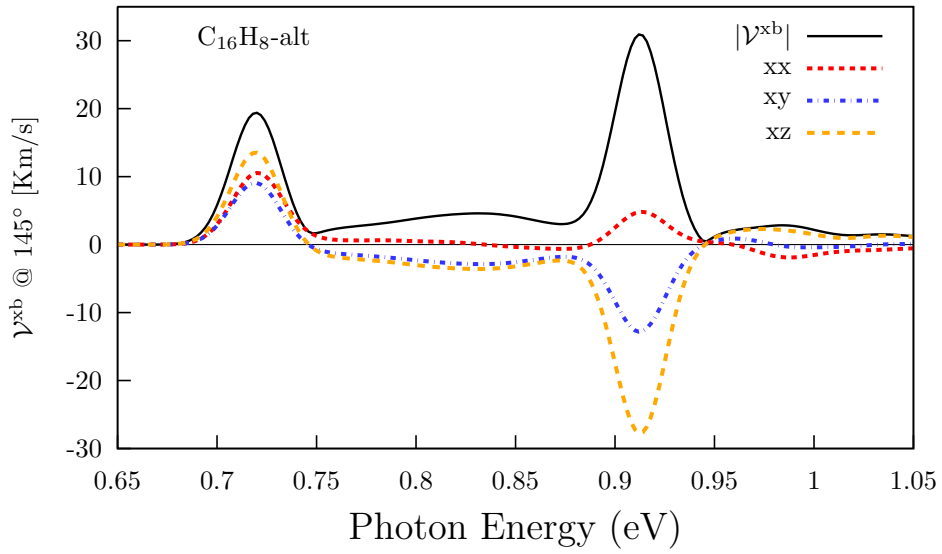

Figure 5: Three components of $\mathcal{V}^{xb}$ @ 145°. fig:alt-vxb1

3.1.2 $\mathcal{V}^{yb}$

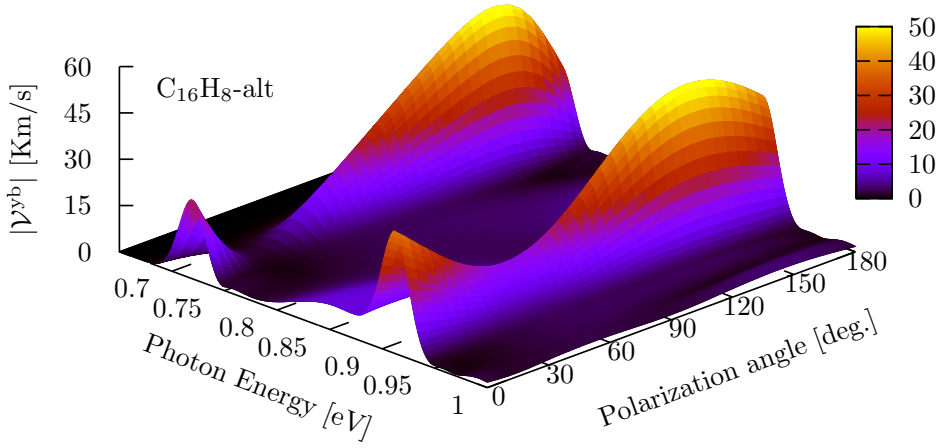

Figure 6: The most intense response for $\mathcal{V}^{\mathrm{yb}}$ is for 145°. fig:alt-magvybincang1

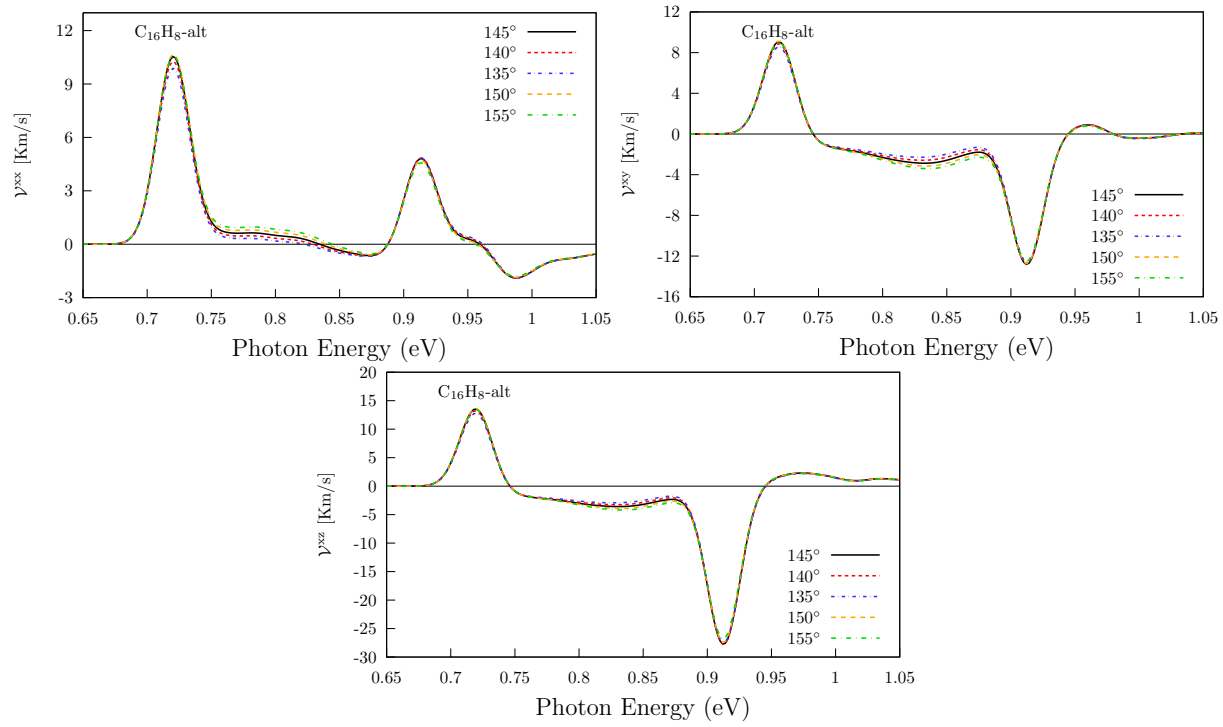

Figure 7: Cheking angle of incidence for *yb* components. fig:alt-ybangcomp

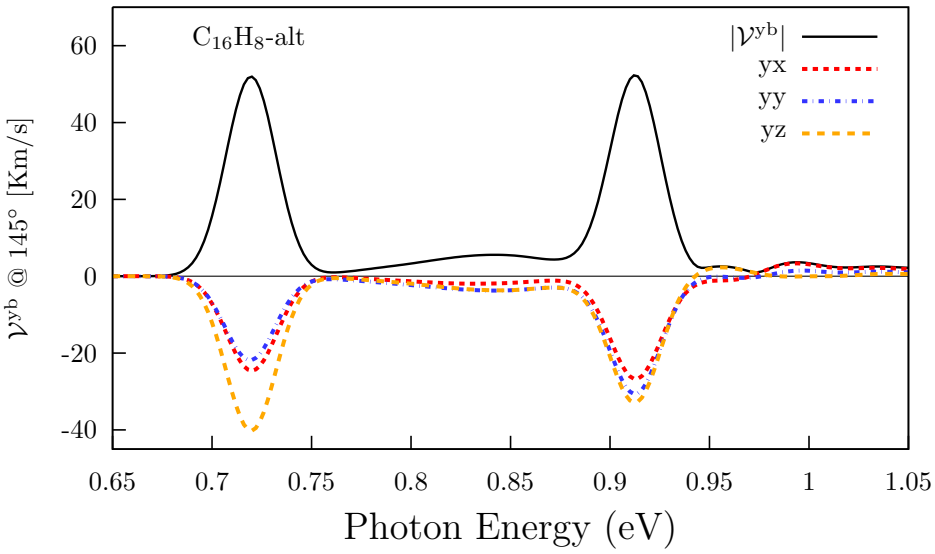

Figure 8: Three components of $\mathcal{V}^{\mathrm{yb}}$ @ 145°.

fig:alt-vyb1

3.1.3 $|\mathcal{V}^{ab}|$, angles θ and φ, layers, and comparison with CdSe and GaAs.

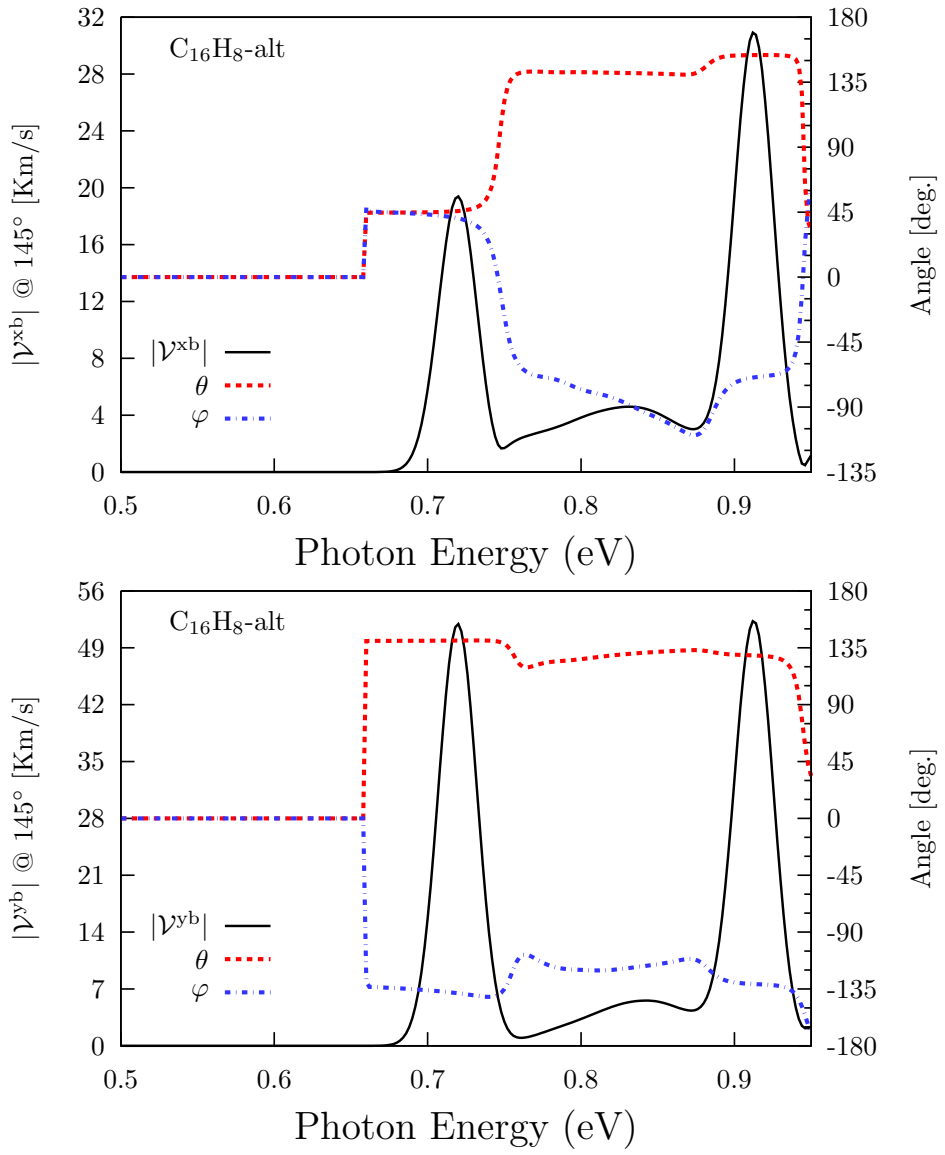

Figure 9: $|\mathcal{V}^{ab}|$ (solid line, leftside scale) and the corresponding angles θ and φ (dashed lines, rightside scale). `fig:alt_rtp`

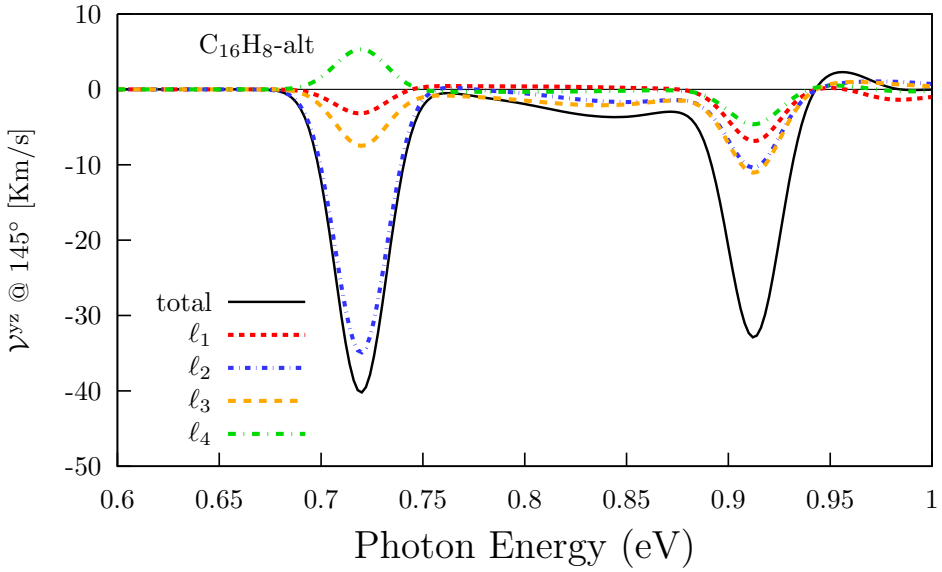

Figure 10: Layer decomposition for the most intense response: $\mathcal{V}^{yz}$. fig:alt-lay

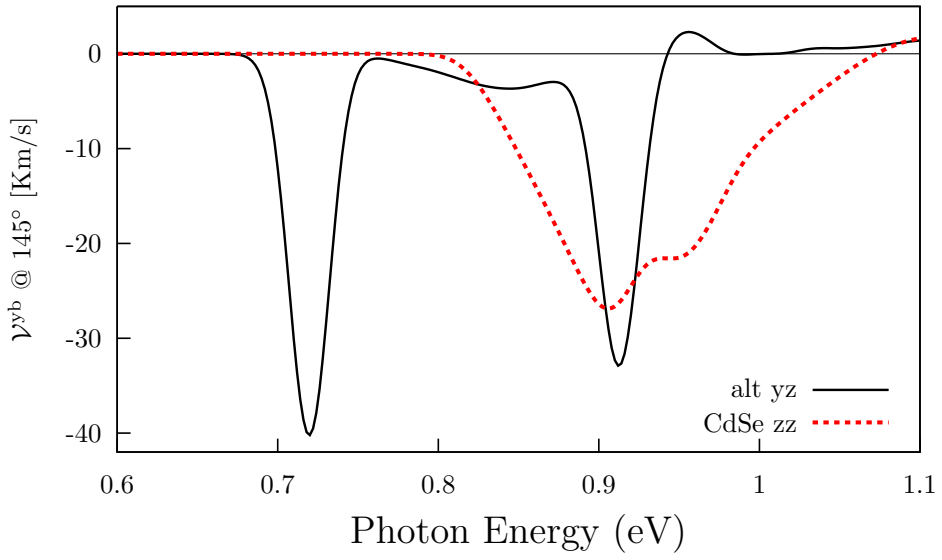

Figure 11: Comparisson of the most intense response vs the most intense responses of CdSe and GaAs. fig:alt-comp

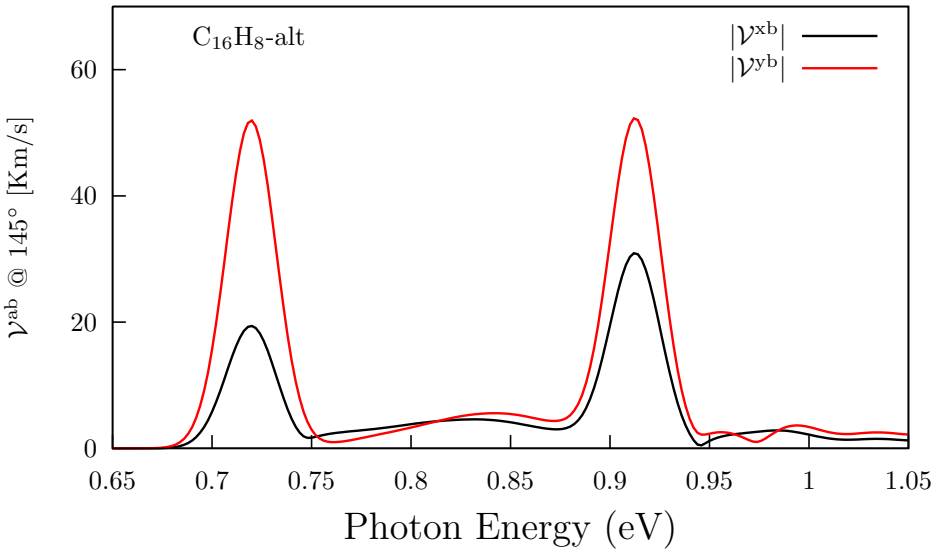

Figure 12: Comparisson of $|\mathcal{V}^{\mathrm{xb}}|$ and $|\mathcal{V}^{\mathrm{yb}}|$ fig:alt-xbybcomp

3.2 Up (graphone)

sec:results-up

3.2.1 $\mathcal{V}^{xb}$ energy range 0.0–0.2 eV

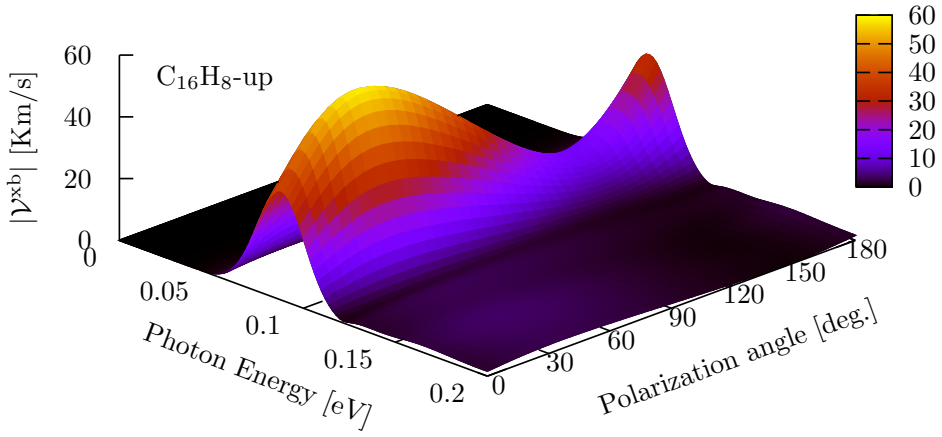

Figure 13: The most intense response for $\mathcal{V}^{xb}$ is for 40°.

fig:up-magvxbincang1

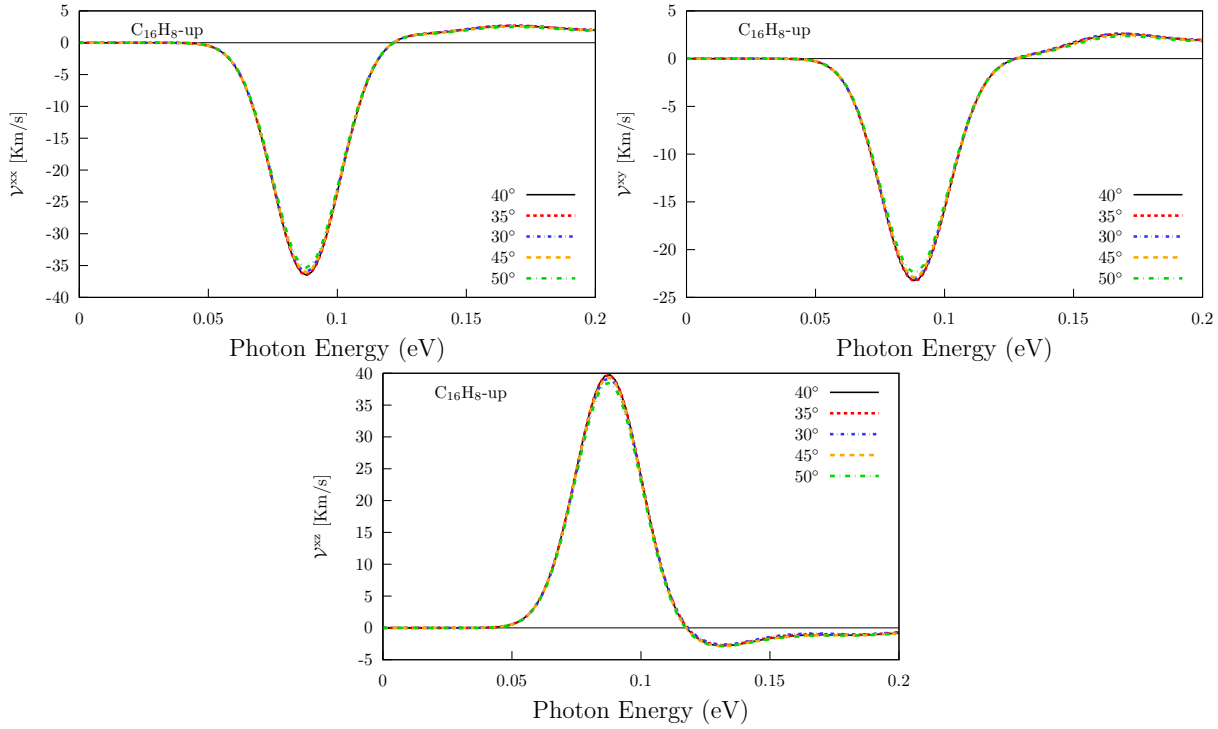

Figure 14: Cheking angle of incidence for xb components for up structure.

fig:up-xbangcomp

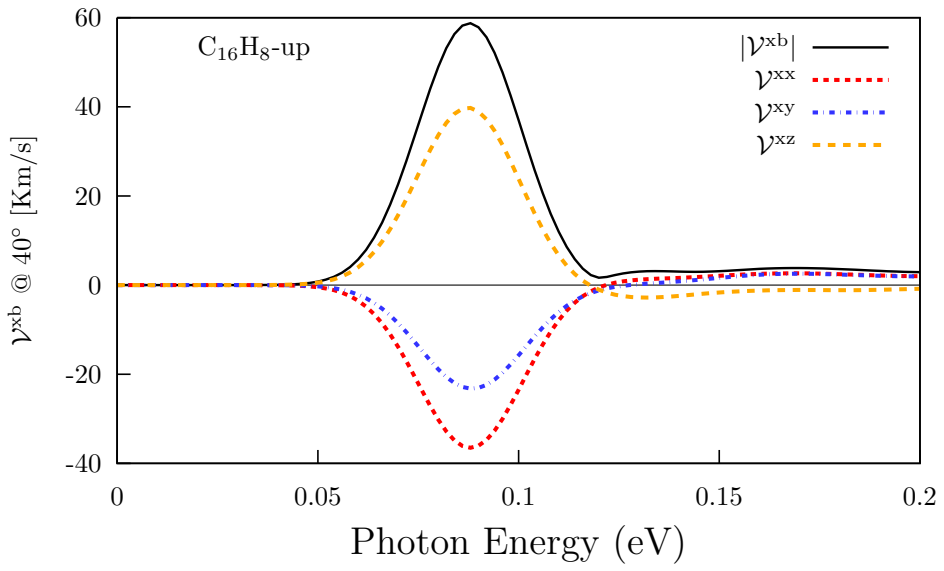

Figure 15: Three components of $\mathcal{V}^{\mathrm{xb}}$ @ 40°. fig:up-vxb1

3.2.2 $\mathcal{V}^{\mathrm{yb}}$ energy range 0.0–0.2 eV

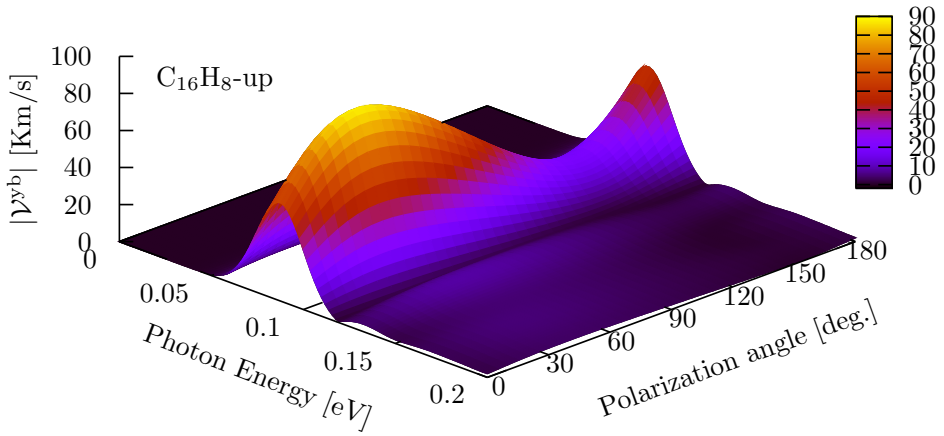

Figure 16: The most intense response for $\mathcal{V}^{\mathrm{yb}}$ is for 40°. fig:up-magvybincang1

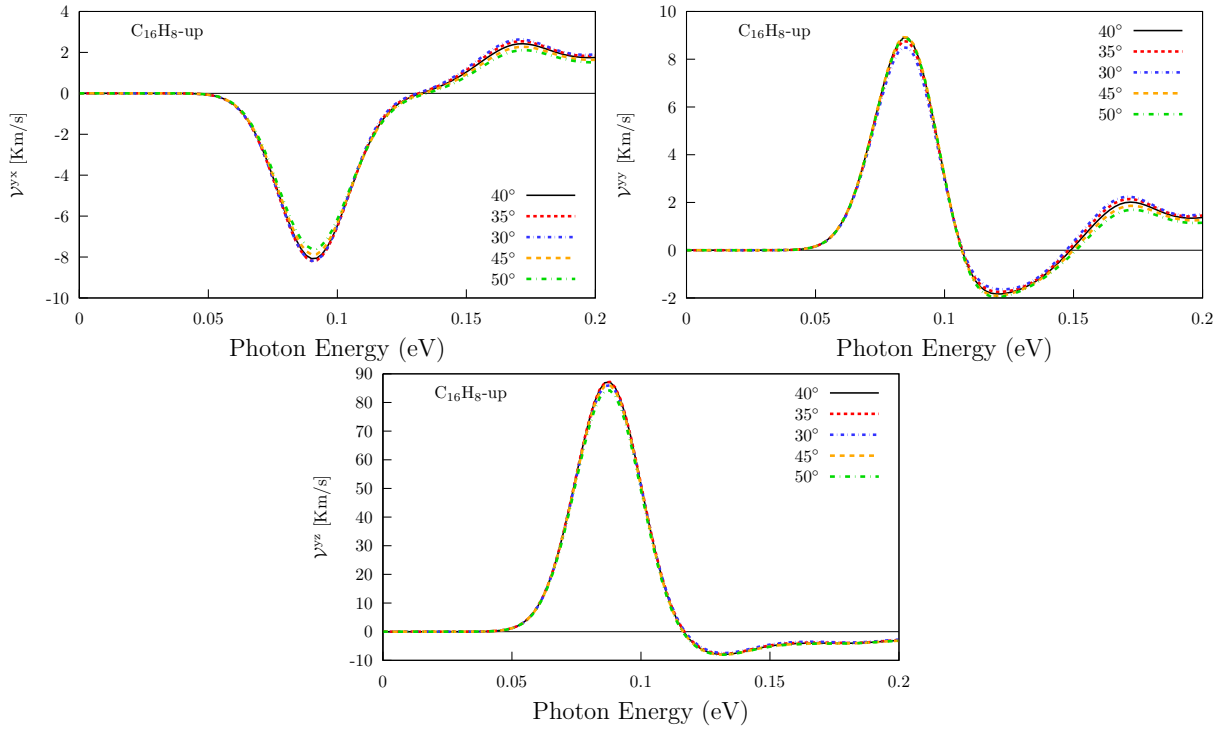

Figure 17: Cheking angle of incidence for *yb* components. `fig:up-ybangcomp`

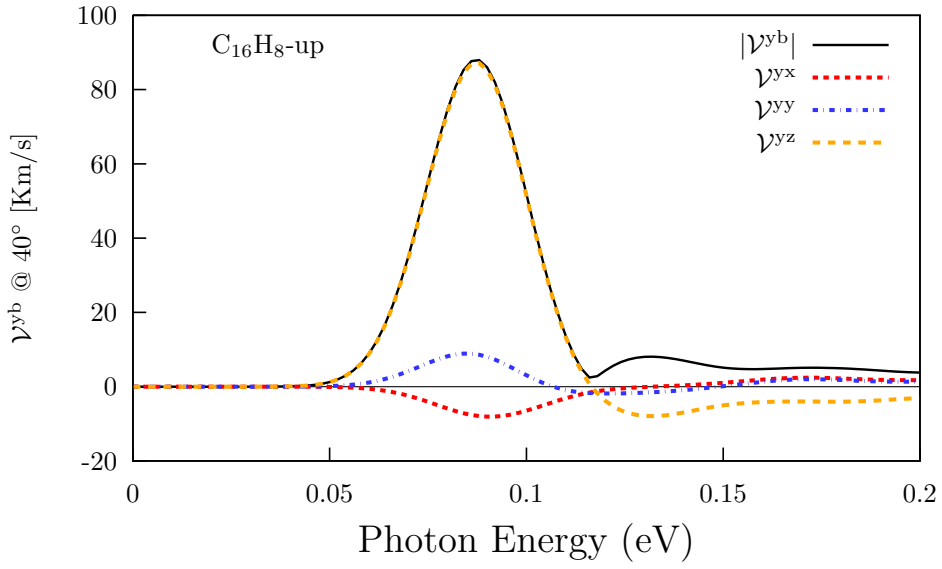

Figure 18: Three components of $\mathcal{V}^{yb}$ @ 40°. `fig:up-vyb1`

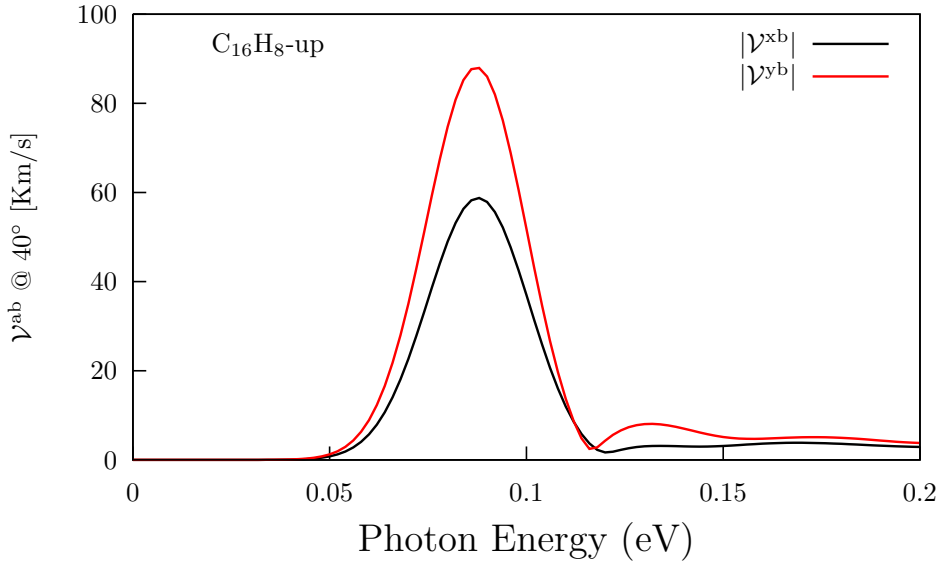

Figure 19: Comparisson of $|\mathcal{V}^{xb}|$ and $|\mathcal{V}^{yb}|$ `fig:up-xbybcomp-1`

3.2.3 $\mathcal{V}^{xb}$ energy range 1.8–2.1 eV

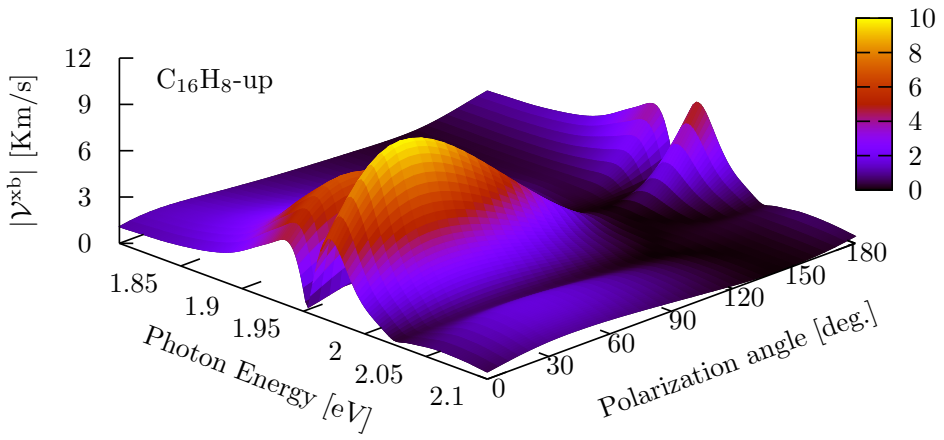

Figure 20: The most intense response for $\mathcal{V}^{xb}$ is for 40°. fig:up-magxbincang2

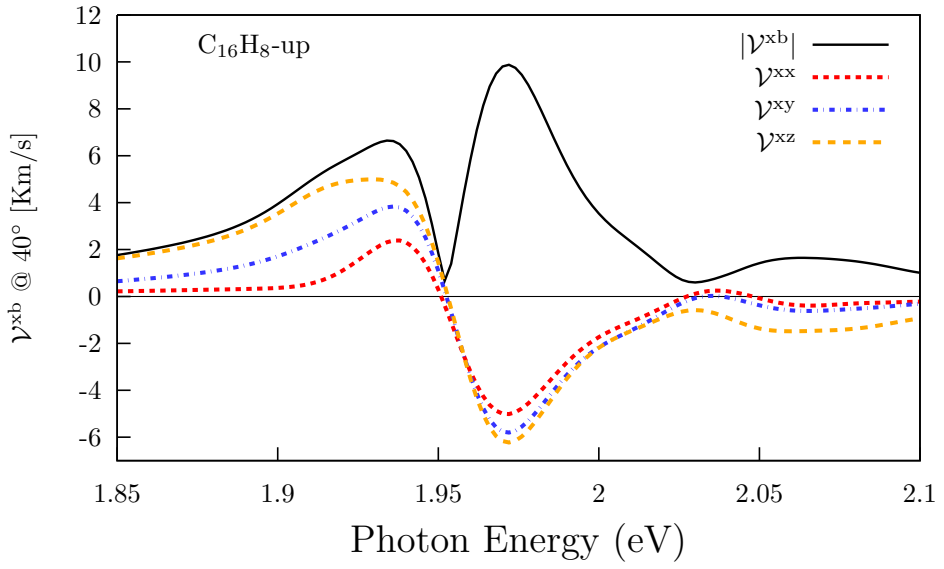

Figure 21: Three components of $\mathcal{V}^{xb}$ @ 40°. fig:up-vxb2

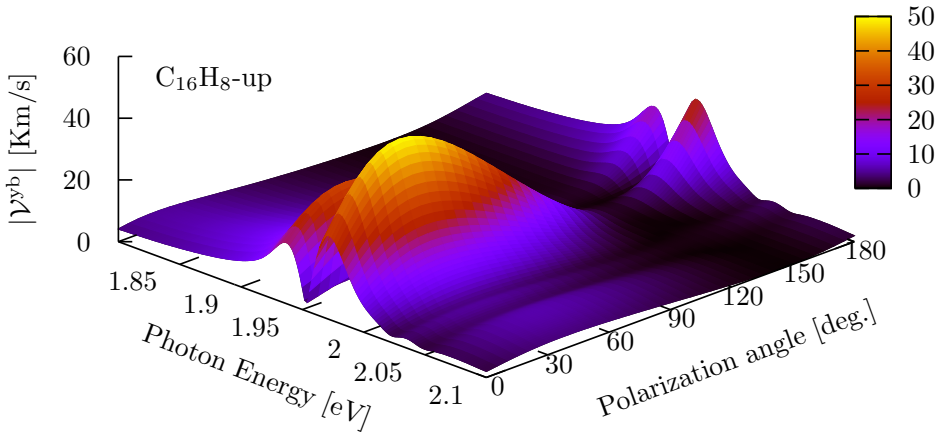

Figure 22: The most intense response for $\mathcal{V}^{\mathrm{yb}}$ is for 40°. fig:up-magybincang2

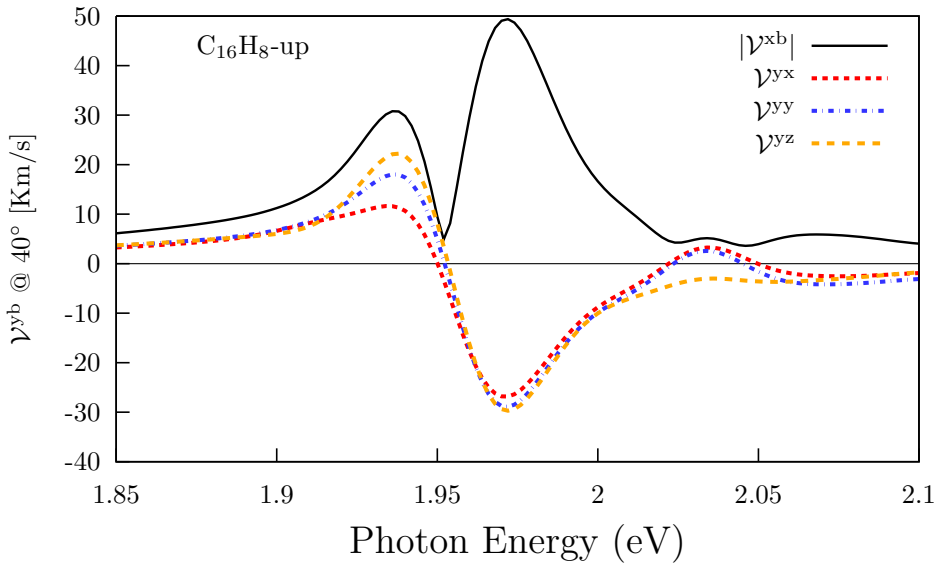

Figure 23: Three components of $\mathcal{V}^{\mathrm{yb}}$ @ 40°. fig:upvyb2

3.2.4 $|\mathcal{V}^{ab}|$, angles θ and φ, layers, and comparison with CdSe and GaAs for the energy range of 0.0–0.2 eV.

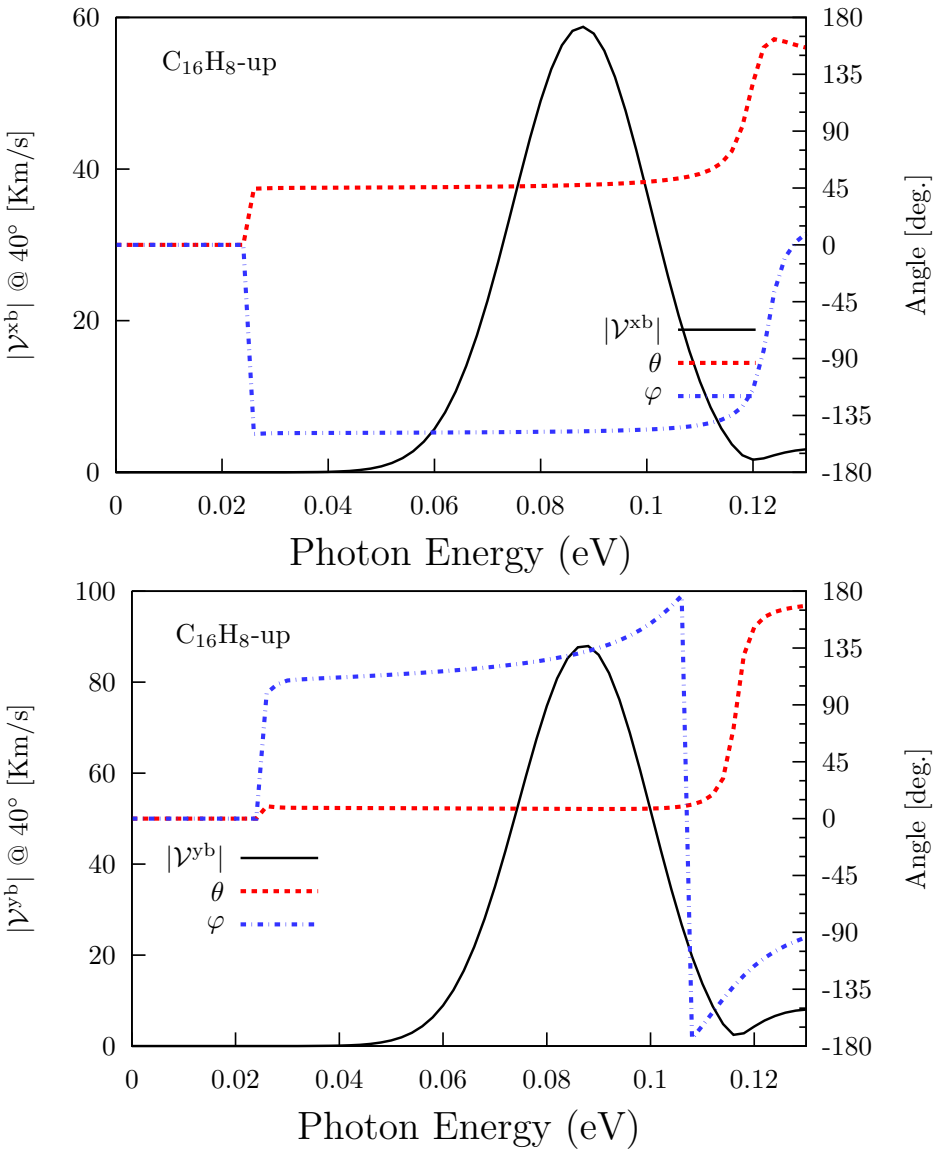

Figure 24: $|\mathcal{V}^{ab}|$ (solid line, leftside scale) and the corresponding angles θ and φ (dashed lines, rightside scale). `fig.up-rtp1`

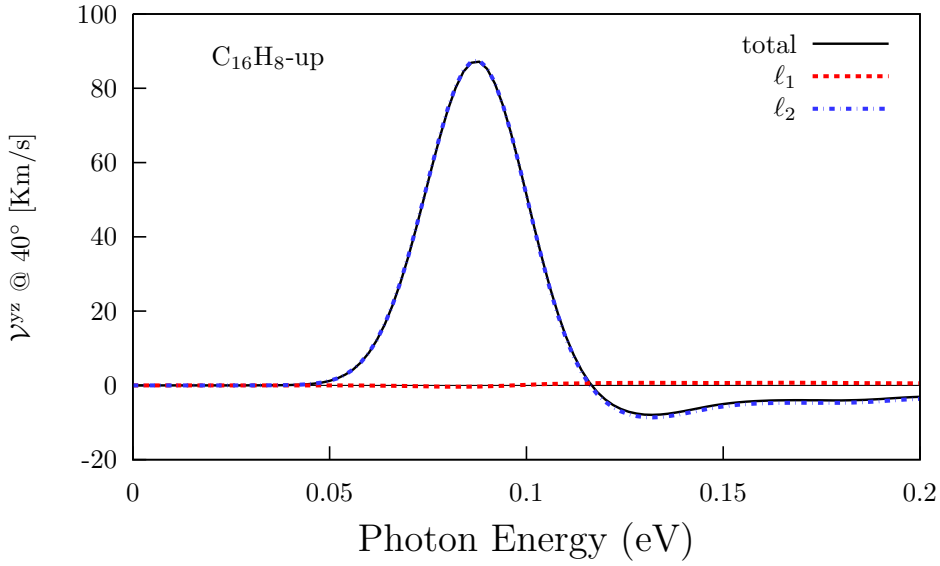

Figure 25: Layer decomposition for the most intense response: $\mathcal{V}^{yz}$. fig:up-lay1

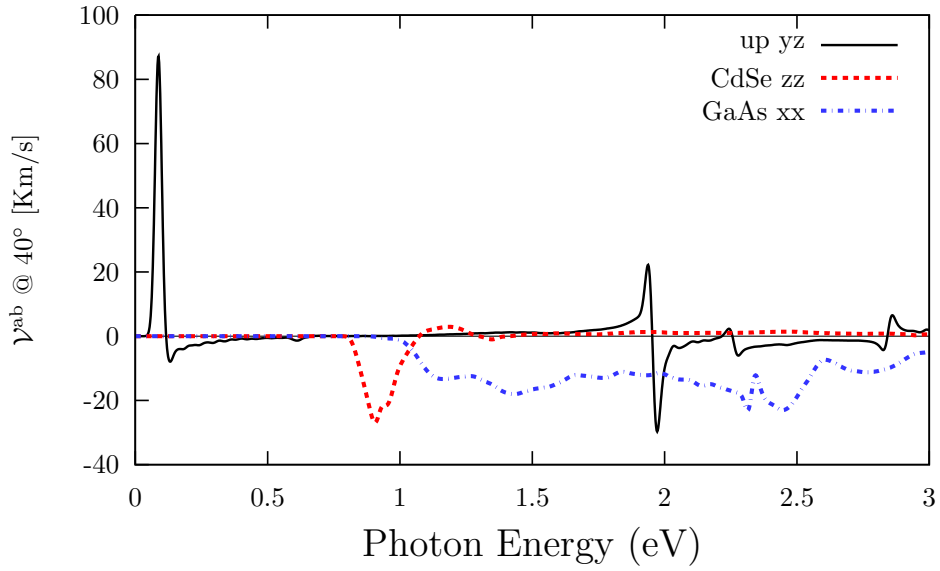

Figure 26: Comparisson of the most intense response vs the most intense responses of CdSe and GaAs. fig:up-comp1

3.2.5 $|\mathcal{V}^{ab}|$, angles θ and φ, layers, and comparison with CdSe and GaAs for the energy range of 1.8–2.1 eV

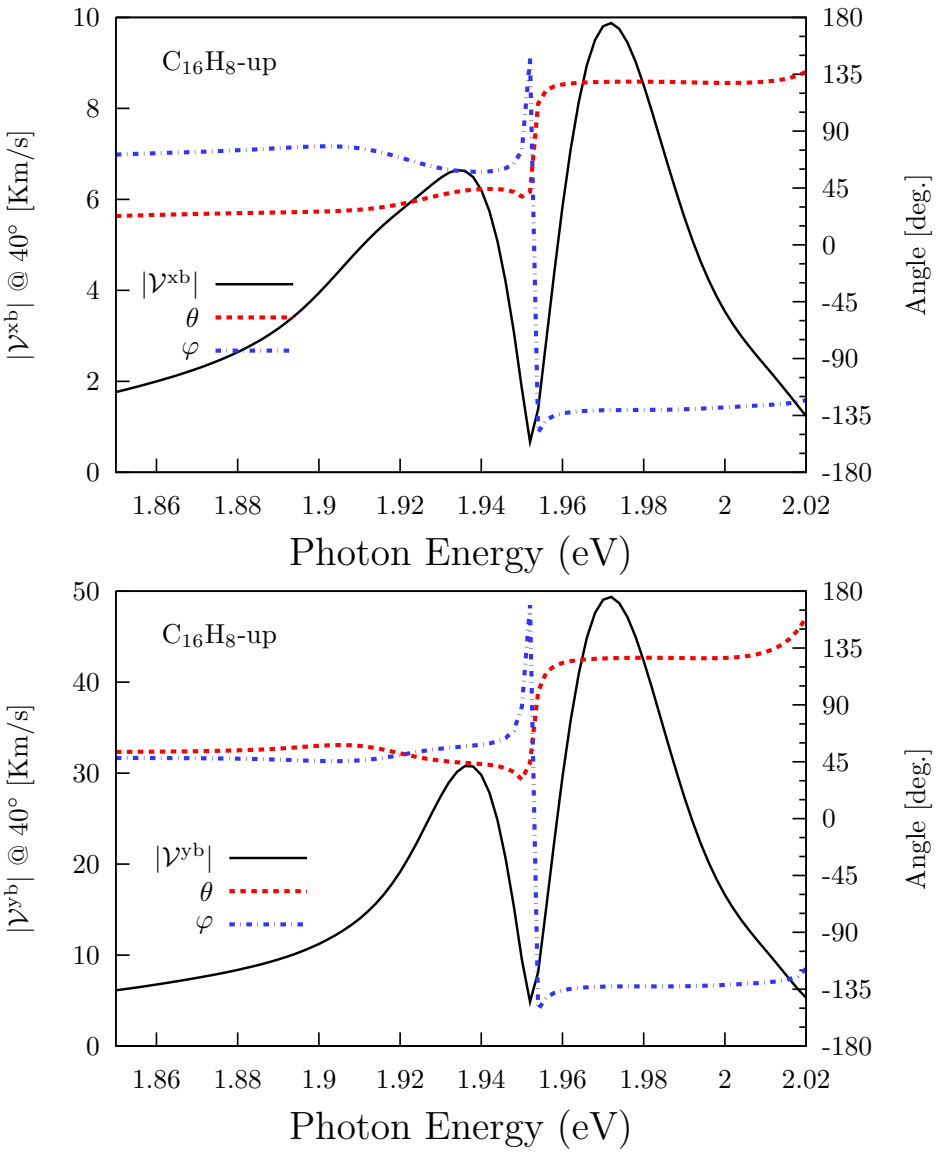

Figure 27: $|\mathcal{V}^{ab}|$ (solid line, leftside scale) and the corresponding angles θ and φ (dashed lines, rightside scale). `fig.up-rtp2`

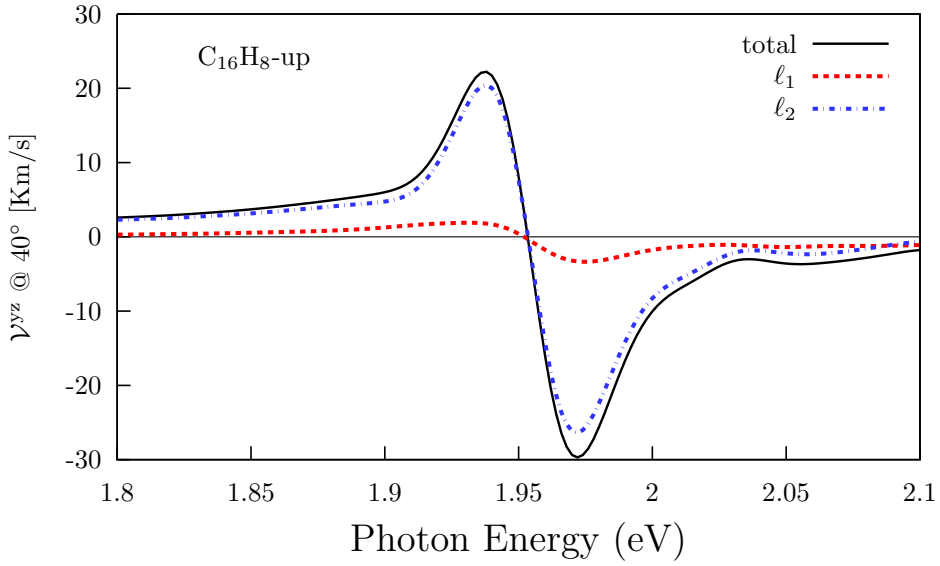

Figure 28: Layer decomposition for the most intense response: $\mathcal{V}^{yz}$. fig:up-lay2

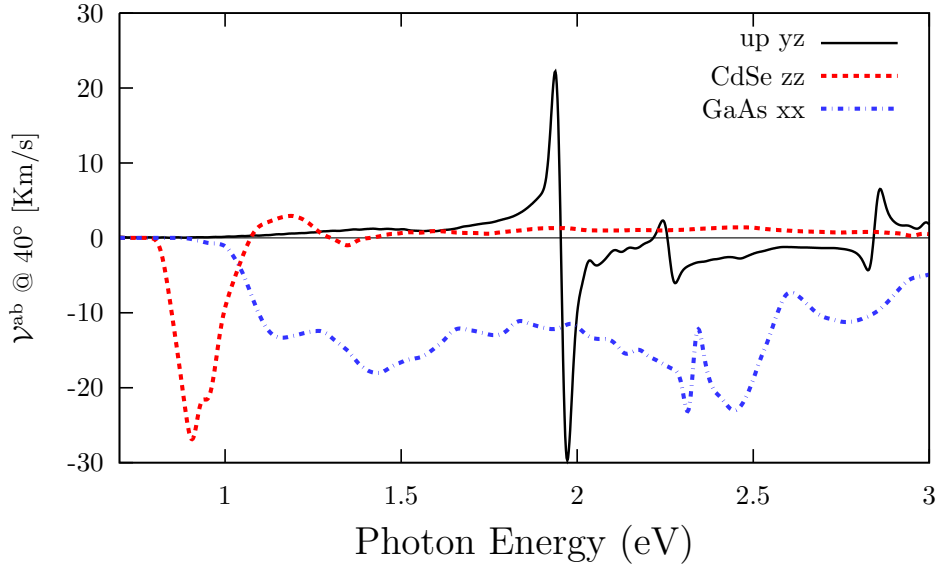

Figure 29: Comparisson of the most intense response vs the most intense responses of CdSe and GaAs. fig:up-comp2

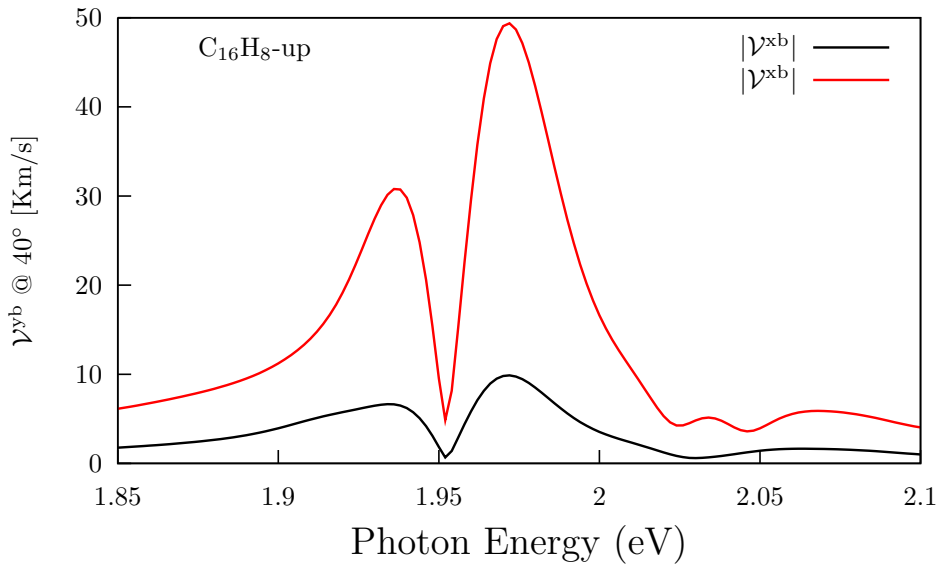

fig:up-xbybcomp-2

References

[1] X. Gonze, B. Amadon, P.-M. Anglade, J.-M. Beuken, F. Bottin, P. Boulanger, F. Bruneval, D. Caliste, R. Caracas, M. Côté, T. Deutsch, L. Genovese, Ph. Ghosez, M. Giantomassi, S. Goedecker, D.R. Hamann, P. Hermet, F. Jollet, G. Jomard, S. Leroux, M. Mancini, S. Mazevet, M.J.T. Oliveira, G. Onida, Y. Pouillon, T. Rangel, G.-M. Rignanese, D. Sangalli, R. Shaltaf, M. Torrent, M.J. Verstraete, G. Zerah, and J.W. Zwanziger. Abinit: First-principles approach to material and nanosystem properties. *Comput. Phys. Commun.*, 180(12):2582–2615, 2009.

[2] C. Hartwigsen, S. Goedecker, and J. Hutter. Relativistic separable dual-space gaussian pseudopotentials from h to rn. *Phys. Rev. B*, 58(7):3641, 1998.

[3] G. Onida, L. Reining, and A. Rubio. Electronic excitations: density-functional versus many-body greens-function approaches. *Rev. Mod. Phys.*, 74(2):601, 2002.

[4] Reinaldo Zapata-Peña, Sean M Anderson, Bernardo S Mendoza, and Anatoli I Shkrebtii. Nonlinear optical responses in hydrogenated graphene structures. *physica status solidi (b)*, 253(2):226–233, 2016.